Implications of $\mathscr{B}(\mu \to e\gamma)$ and Δa_μ on Muonic Lepton Flavor Violating Processes

Chun-Khiang CHUA[*]

Chung Yuan Christian University
E-mail: ckchua@cycu.edu.tw

We study the implications of the experimental results on the $\mu \to e\gamma$ decay rate and the muon anomalous magnetic moment, on muonic lepton flavor violating processes, such as $\mu \to 3e$ and $\mu N \to eN$. We use a model-independent approach in this analysis, where these processes are considered to be loop induced by exchanging spin-1/2 and spin-0 particles. We explore two complementary cases–those with no cancellation mechanism in amplitudes and those with an internal (built-in) cancellation mechanism. Our main results are as follows: (a) Bounds from rates are used to constrain parameters, such as coupling constants and masses. These constraints can be easily updated by simple scalings, if the experimental situations change. (b) The muon $g-2$ data favor nonchiral interactions. (c) In $\mu \to 3e$ and $\mu N \to eN$ processes, Z-penguin diagrams may play some role, while box diagram contributions to $\mu \to 3e$ are usually highly constrained. (d) In the first case (without any built-in cancellation mechanism), using the recent $\mu \to e\gamma$ bound, we find that $\mu \to 3e$ and $\mu N \to eN$ rates are usually bounded below the present experimental limits by two to three orders of magnitude in general. Furthermore, by comparing Δa_μ and $\mathscr{B}(\mu \to e\gamma)$ data, the couplings of μ and e are found to be highly hierarchical. Additional suppression mechanisms should be called for. (e) In the second case (with a built-in cancellation mechanism), mixing angles can provide additional suppression factors to satisfy the Δa_μ and $\mathscr{B}(\mu \to e\gamma)$ bounds. While the $\mu \to 3e$ rate remains suppressed, the bounds on $\mu N \to eN$ rates, implied from the latest $\mu \to e\gamma$ bound, can be relaxed significantly and can be just below the present experimental limits.

---

[*]Speaker.

1. Introduction

Charge lepton flavor violating (LFV) processes are prohibited in the Standard Model (SM) and, hence, are excellent probes of New Physics (NP). Recently the search of $\mu \to e\gamma$ decay was reported by the MEG collaboration giving [1] $\mathscr{B}(\mu^+ \to e^+\gamma) \leq 2.4 \times 10^{-12}$. The bound is several times lower than the previous one [2]. In many New Physics models this decay mode is closely related to other lepton flavor violating processes, such as $\mu^+ \to e^+e^+e^-$ decays and $\mu^- N \to e^- N$ conversions [3]. The present limits and future experimental sensitivities [1, 2, 4] of these LFV processes are summarized in Table 1. Note that present bounds on μ LFV rates are roughly of similar orders. It will be interesting to see what the implications are of the new $\mathscr{B}(\mu \to e\gamma)$ bound on these LFV processes and the interplay between them [5].

Since 2001, the muon anomalous magnetic moment remains as a hint of a NP contribution (see, for a review, [6]). Experimental data deviates from the Standard Model (SM) expectation by more than 3σ [2]: $\Delta a_\mu = a_\mu^{\mathrm{exp}} - a_\mu^{\mathrm{SM}} = (287 \pm 63 \pm 49) \times 10^{-11}$. Since NP contributes to Δa_μ and $\mathscr{B}(\mu^+ \to e^+\gamma)$ through very similar loop diagrams [see Fig. 1(a) and (b)], it is useful to compare them at the same time.

We consider a class of models that muon $g - 2$ and various muon lepton flavor violating processes, such as $\mu \to e\gamma$, $\mu \to 3e$ and $\mu \to e$ conversions, are loop-induced by exchanging spin-1/2 and spin-0 particles [5]. We try to see where the present $g - 2$ and $\mu \to e\gamma$ experimental results lead us on estimating rates or bounds on various LFV muonic decay modes and the interplay between them. Two cases, which are complementary to each other, are considered. In the first case (Case I), there is no built-in cancellation mechanism among amplitudes. The second case (Case II) is with some built-in mechanism, such as GIM or super GIM mechanism.

2. Results: Case I

We start with Case I. In Fig. 2 we show the allowed parameter space for $Q_{\phi,\psi}|g_{\mu L(R)}|^2/m_\psi^2$ and $Q_{\phi,\psi}\mathrm{Re}(g_{\mu R}^*g_{\mu L})/m_\psi$ ($g_{lL(R)}$ are couplings of ϕ–ψ–$l_{L(R)}$ interactions) constrained by the measured Δa_μ with exclusion of $|g_{\mu L(R)}|^2, |g_{\mu L}g_{\mu R}| > 4\pi$ and $m_{\psi,\phi} < 100$ GeV. The latter requirements are to ensure perturbativity and to satisfy the experimental bounds on the masses of exotic particles [2]. Bands denoted with ϕ or ψ are allowed regions obtained through contributions from diagrams with ϕ or ψ interacting with a photon [see Fig 1(a) and (b)]. From Fig. 2(a), we see that the allowed regions on $Q_\phi|g_{\mu L(R)}|^2/m_\psi^2$ and $-Q_\psi|g_{\mu L(R)}|^2/m_\psi^2$ are similar and the signs of $Q_{\phi,\psi}$ are constrained by data. Note that the allowed parameter space is quite limited and is almost closed by the bounds

Table 1: Current experimental upper limits and future sensitivities on various μ LFV processes [1, 2, 4].

|	current limit	future sensitivity
$\mathscr{B}(\mu^+ \to e^+\gamma)$	$< 2.4 \times 10^{-12}$	10^{-13}
$\mathscr{B}(\mu^+ \to e^+e^+e^-)$	$< 1.0 \times 10^{-12}$	$10^{-14} - 10^{-16}$
$\mathscr{B}(\mu^-\mathrm{Ti} \to e^-\mathrm{Ti})$	$< 4.3 \times 10^{-12}$	10^{-18}
$\mathscr{B}(\mu^-\mathrm{Au} \to e^-\mathrm{Au})$	$< 7 \times 10^{-13}$	$10^{-14} - 10^{-16}$
$\mathscr{B}(\mu^-\mathrm{Al} \to e^-\mathrm{Al})$	$\cdots$	10^{-16}
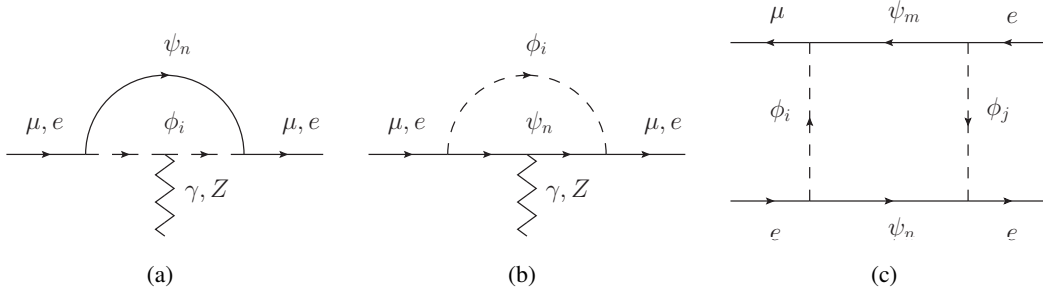
Figure 1: (a) and (b): Penguin diagrams that contribute to muon $g-2$, $\mu^+ \to e^+\gamma$, $\mu^+ \to e^+e^+e^-$ and $\mu^-N \to e^-N$ processes. Note that diagrams involving self energy parts are not shown. (c) : Box diagram contributing to the $\mu^+ \to 3e$ process. Another diagram is needed when $\psi_{m,n}$ are Majorana fermions.

from $|g_{\mu L(R)}|^2 < 4\pi$ and $m_\psi > 100\,\mathrm{GeV}$ and $m_\phi > 100\,\mathrm{GeV}$. Thus, it is unlikely to use a chiral-type interaction to generate the measured Δa_μ. From Fig. 2(b), we see that the allowed parameter space is substantially larger. We now turn to μ LFV processes, including $\mu \to e\gamma$, $\mu \to 3e$, $\mu\mathrm{Ti} \to e\mathrm{Ti}$ and $\mu\mathrm{Au(Al)} \to e\mathrm{Au(Al)}$ transitions. In Fig. 2(c) and (d), we show the parameter space excluded by various bounds and the one corresponding to projections from the expected sensitivities on these μ LFV processes, through contributions from photonic diagrams. In Fig. 2(e) and (f) rate ratios of various modes through photonic penguins are given. Since the present experimental bounds on LFV rates are of similar orders of magnitudes (see Table 1), the present bound on the $\mu \to e\gamma$ rate provides the most severe constraint. We find that $\mu \to 3e$ and $\mu^-N \to e^-N$ rates are bounded below the present experimental limits by two to three orders of magnitude in general.

Since NP contributions to Δa_μ and the $\mu^+ \to e^+\gamma$ decay are from similar diagrams, it will be useful to compare them. We find that the present data on Δa_μ and $\mathscr{B}(\mu^+ \to e^+\gamma)$ lead to $\frac{g_{\mu R(L)}g_{eL(R)}}{g_{\mu R}g_{\mu L}} = \frac{g_{eL(R)}}{g_{\mu L(R)}} \leq 4.2 \times 10^{-5} \simeq \lambda^6$, where we define $\lambda \equiv 0.2$. This ratio is much smaller than any known coupling ratio and mixing angle among the first and second generations. It seems that the present case is unnatural.

3. Results: Case II

We now turn to Case II. Results are shown in Fig. 3 (note that δ is a mixing angle of ϕ). Fig. 3(a) is same as Fig. 2(a). Comparing Fig. 3(b) to Fig. 2(b), we see that the allowed parameters in the upper m_ϕ/m_ψ region are similar. In contrast, they are relaxed substantially in the lower m_ϕ/m_ψ region in the present case. The built-in cancellation mechanism reduces the amplitudes effectively and a too heavy ψ is incapable to produce a large enough Δa_μ. The effect of the cancellation is important in the low m_ϕ/m_ψ region and, consequently, relaxes the constraints on parameters. In Fig. 3(c) and (d), we show the constrained and projected parameter space through penguin contributions by considering the experimental bounds and the proposed sensitivities. By comparing the constraints from Δa_μ and $\mathscr{B}(\mu \to e\gamma)$ we obtain $\frac{g_{\mu R(L)}g_{eL(R)}\mathrm{Re}[(\delta_{RL(LR)})_{\mu e}]}{g_{\mu R}g_{\mu L}\mathrm{Re}[(\delta_{RL})_{\mu\mu}]} = \frac{g_{eL(R)}}{g_{\mu L(R)}}\frac{\mathrm{Re}[(\delta_{RL(LR)})_{\mu e}]}{\mathrm{Re}[(\delta_{RL})_{\mu\mu}]} \leq 4.2 \times 10^{-5} \simeq \lambda^6$. If we estimate $g_{eL(R)}/g_{\mu L(R)}$ by using the lepton mass ratio $m_e/m_\mu \sim \lambda^{3\sim4}$, we see that a mixing angle ratio of $\mathrm{Re}[(\delta_{RL(LR)})_{\mu e}]/\mathrm{Re}[(\delta_{RL})_{\mu\mu}] \lesssim \lambda^{2\sim3}$, which is not unnatural, can easily satisfy the above bound. In this respect, case II is more reasonable and natural than case I, where the
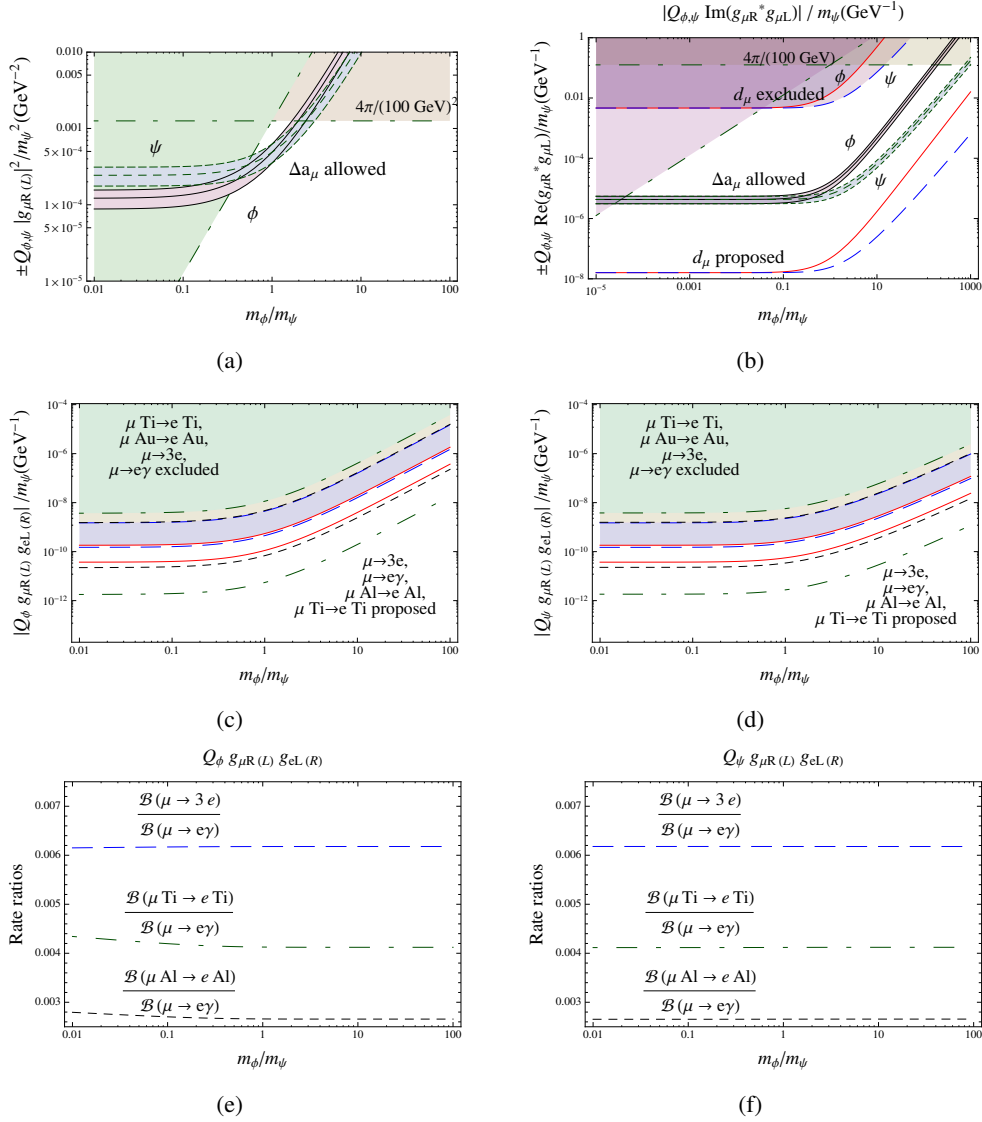
Figure 2: (a), (b): Allowed parameter space for $\pm Q_{\phi,\psi}|g_{\mu L(R)}|^2/m_\psi^2$ and $\pm Q_{\phi,\psi}\text{Re}(g_{\mu R}^* g_{\mu L})/m_\psi$ constrained by Δa_μ. (c), (d): Parameter space excluded (projected) by various bounds (expecting sensitivities) on μ LFV processes through contributions from photonic penguins. (e), (f): Ratios of rates contributed from photonic penguins.

coupling ratio is highly hierarchical. It is interesting to see from Fig. 3 (c) and (d) that the $\mu \to e\gamma$ bound is not always the most stringent one. For example, comparing Fig. 3(c) with Fig. 2(c), we see that in the low m_ϕ/m_ψ region both bounds from $\mu \to e\gamma$ and $\mu \to 3e$ are relaxed up to three orders of magnitude, while the changes on those from $\mu N \to eN$ are mild. We can infer that, similar to the Δa_μ case, the F_2 (photonic) penguin amplitudes exhibit cancellations in amplitudes in the low m_ϕ/m_ψ region and relax the constraints from $\mu \to e\gamma$ significantly, while the cancellations in the F_1 penguin contributions in $\mu \to 3e$ and $\mu N \to eN$ processes are mild. As a result the bounds from $\mu N \to eN$ approach the $\mu \to e\gamma$ bound in this case, while in the previous case these two bounds are always apart. The ratios of photonic penguin contributing rates plotted in Fig. 3(e) and (f) show
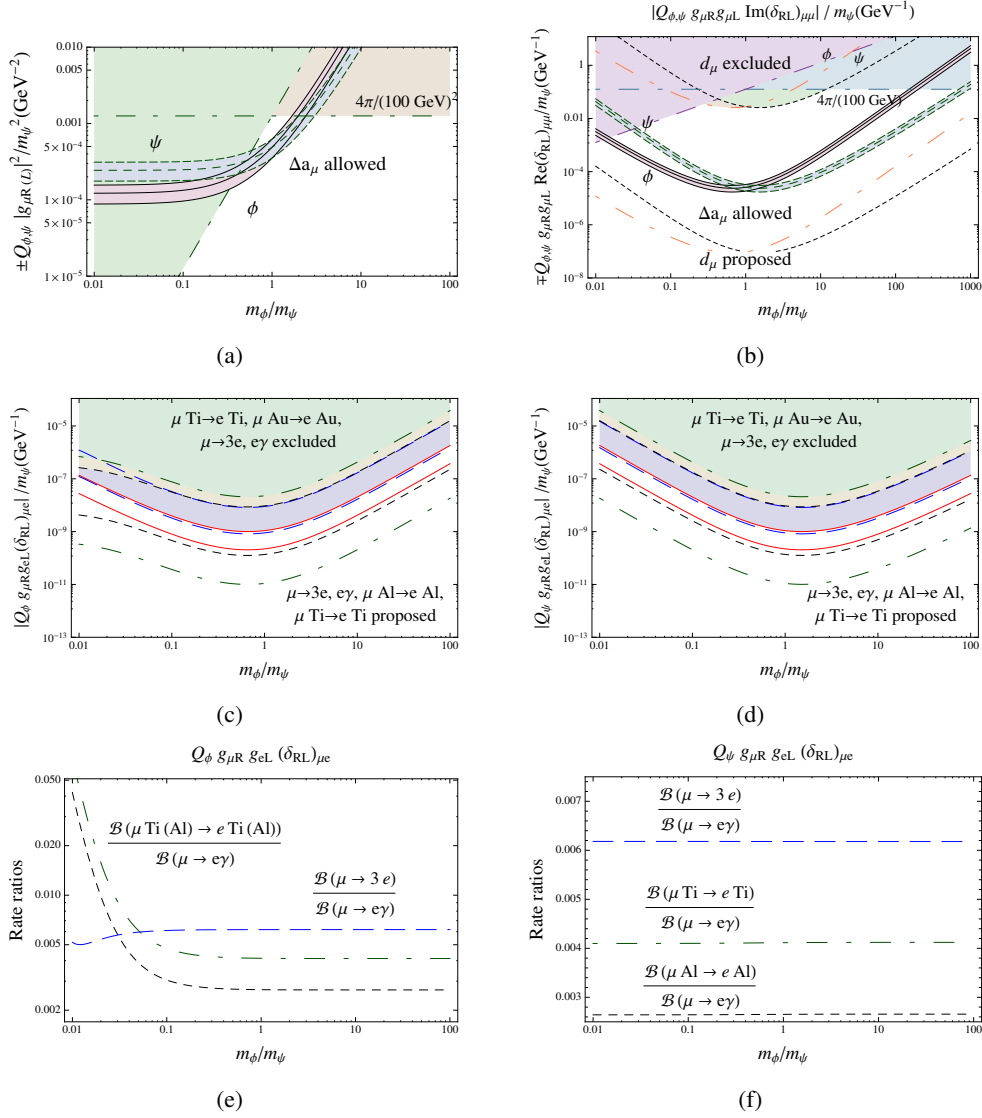
Figure 3: Same as Fig. 2, but in Case II.

that $\mathscr{B}(\mu N \to eN)/\mathscr{B}(\mu \to e\gamma)$ and $\mathscr{B}(\mu \to 3e)/\mathscr{B}(\mu \to e\gamma)$ are enhanced compared with those in Fig. 2(e) and (f). In Fig. 3(e) the $\mathscr{B}(\mu N \to eN)/\mathscr{B}(\mu \to e\gamma)$ ratio is enhanced by one order of magnitude, while the $\mathscr{B}(\mu \to 3e)/\mathscr{B}(\mu \to e\gamma)$ ratio does not change much. It is very interesting that the rate ratio $\mathscr{B}(\mu N \to eN)/\mathscr{B}(\mu \to e\gamma)$ from the $g_{\mu R(L)}g_{eL(R)}$ term is enhanced and different from Case I. We find that the present bound on $\mu \to e\gamma$ allows $\mathscr{B}(\mu N \to eN) \lesssim 10^{-13}$, which is close to the present bounds (see Table 1). Therefore, the search on these processes could be very interesting. In Fig. 4, we show the constraints on parameters which contribute through box diagrams to the $\mu^+ \to 3e$ process in this case. Note that constraints on the same combinations of parameters can be obtained from penguin processes, including $\mu \to e\gamma$, Δa_e, EDM, and the purturbative bounds, as well. We see that these constraints are usually much stronger than the ones from the box diagrams. Hence, in general, these box diagrams do not play a major role in the $\mu^+ \to 3e$ decay. Results from Z exchange can be found in Ref. [5].
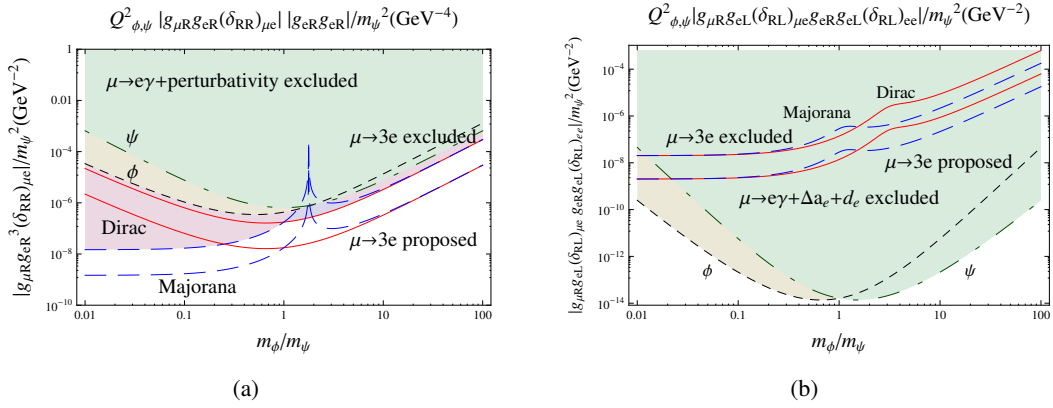
Figure 4: Constraints on parameters which contribute through box diagrams to the $\mu \to 3e$ process.

4. Conclusion

In conclusion, we use a model independent approach in this analysis, where these processes are considered to be loop-induced by exchanging spin-1/2 and spin-0 particles [5]. We explore two complementary cases, without or with an internal (built-in) cancellation mechanism in amplitudes. Our main results are as follows: (a) Bounds from rates are used to constrain parameters, such as coupling constants and masses. (b) The muon $g-2$ data favor nonchiral interactions. (c) In $\mu \to 3e$ and $\mu^- N \to e^- N$ processes, the Z-penguin diagrams may play some role, while the box diagram contributions to the $\mu \to 3e$ rate are usually highly constrained. (d) In the first case (without any built-in cancellation mechanism), using the recent $\mu^+ \to e^+ \gamma$ bound, we find that $\mu \to 3e$ and $\mu^- N \to e^- N$ rates are bounded below the present experimental limits by two to three orders of magnitude in general. Furthermore, by comparing Δa_μ and $\mathcal{B}(\mu \to e\gamma)$ data, the couplings of g_μ and g_e are found to be highly hierarchical. Additional suppression mechanisms should be called for. (e) In the second case (with a built-in cancellation mechanism), mixing angles can provide additional suppression factors to satisfy the Δa_μ and $\mathcal{B}(\mu \to e\gamma)$ bounds without relaying only on highly hierarchical g_e and g_μ couplings. In addition, although the $\mu \to 3e$ rate remains suppressed, the bounds on $\mu^- N \to e^- N$ rates, implicated by the MEG $\mu^+ \to e^+ \gamma$ bound, can be relaxed significantly in the second case and can be just below the present experimental limits.

References

[1] J. Adam *et al.* [MEG Collaboration], Phys. Rev. Lett. **107**, 171801 (2011).

[2] K. Nakamura *et al.* [Particle Data Group Collaboration], J. Phys. G **37**, 075021 (2010).

[3] Y. Kuno and Y. Okada, Rev. Mod. Phys. **73**, 151 (2001).

[4] Y. Kuno, PoS FPCP **2010**, 049 (2010); M. De Gerone and M. E. G. Collaboration, arXiv:1108.2670; T. Nomura, talk given at FPCP 2011; B. Casey, *ibid.*; A. Hoecker, arXiv:1201.5093.

[5] C. -K. Chua, Phys. Rev. D **86**, 093009 (2012).

[6] F. Jegerlehner and A. Nyffeler, Phys. Rept. **477**, 1 (2009).